Journal of Crystal Growth 408 (2014) 97–101

Contents lists available at ScienceDirect

Journal of Crystal Growth

journal homepage: www.elsevier.com/locate/jcrysgro

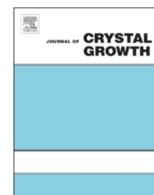

Structural and optical properties of Ga auto-incorporated InAlN epilayers

E. Taylor [a,*], M.D. Smith [b,c], T.C. Sadler [b], K. Lorenz [d], H.N. Li [b,c], E. Alves [d], P.J. Parbrook [b,c], R.W. Martin [a,*]

[a] Department of Physics, SUPA, University of Strathclyde, Glasgow G4 0NG, United Kingdom
[b] Tyndall National Institute, University College Cork, Lee Maltings, Dyke Parade, Cork, Ireland
[c] School of Engineering, University College Cork, College Road, Cork, Ireland
[d] IPFN, Instituto Superior Técnico, Campus Tecnológico e Nuclear, Universidade de Lisboa, Estrada Nacional 10, P-2695-066 Bobadela LRS, Portugal

ARTICLE INFO

Article history:
Received 26 March 2014
Received in revised form
2 September 2014
Accepted 4 September 2014
Communicated by R. Bhat
Available online 28 September 2014

Keywords:
A1. Ga incorporation
A1. Rutherford backscattering spectrometry
A1. Wavelength dispersive x-ray
A3. Metalorganic chemical vapour deposition
B1. InAlN
B1. InAlGaN

ABSTRACT

InAlN epilayers deposited on thick GaN buffer layers grown by metalorganic chemical vapour deposition (MOCVD) revealed an auto-incorporation of Ga when analysed by wavelength dispersive x-ray (WDX) spectroscopy and Rutherford backscattering spectrometry (RBS). Samples were grown under similar conditions with the change in reactor flow rate resulting in varying Ga contents of 12–24%. The increase in flow rate from 8000 to 24 000 sccm suppressed the Ga auto-incorporation which suggests that the likely cause is from residual Ga left behind from previous growth runs. The luminescence properties of the resultant InAlGaN layers were investigated using cathodoluminescence (CL) measurements.
© 2014 The Authors. Published by Elsevier B.V. This is an open access article under the CC BY license (http://creativecommons.org/licenses/by/3.0/).

1. Introduction

InAlN is a wide and direct bandgap semiconductor alloy spanning an energy range of 0.7–6.2 eV. It has an advantage over other ternary nitride alloys in that it can be lattice matched to GaN with an InN content of ~17%, reducing strain induced defects, which improves crystalline quality and device efficiency [1,2]. This gives InAlN the potential to replace other alloys such as AlGaN and InGaN in optoelectronic and power transistor devices. However difficulty arises in the growth of InAlN (and InAlGaN) due to the temperature differences between InN (~600 °C) and AlN (~1100 °C). This can lead to substantial compositional inhomogeneities and large variations in bandgap [3]. A widely researched application for InAlN is the substitution of AlGaN barrier layers with InAlN in GaN based high electron mobility transistor (HEMT) structures [4–6]. The presence of the InAlN barrier induces a high density two dimensional electron gas (2DEG) through the difference in spontaneous polarisation between InAlN and GaN, allowing for higher current densities. Furthermore, lattice matching the InAlN to GaN helps in reducing barrier stress which in turn may improve device reliability [7]. InAlN can also be used for in situ optical monitoring during metalorganic chemical vapour deposition (MOCVD) growth of GaN based structures on free standing GaN substrates [8]. This application exploits the difference in refractive index of lattice matched InAlN compared to GaN to aid with accurate growth thickness using in situ reflectometry. The inclusion of thin InAlN allows for reflectivity oscillations whilst not inducing extra dislocations.

Recently it has been reported that unintentional Ga incorporation can occur during MOCVD growth of InAlN layers on GaN buffers in close-coupled showerhead vertical MOCVD reactors [9,10]. The Ga incorporation has been associated with leftover trimethylgallium (TMGa) precursor and Ga deposits on the susceptor and reactor walls [9,11]. Another proposed cause is diffusion of Ga from the underlying GaN layer [10]. Unwanted Ga incorporation can change the structural, electrical and optical properties of the nominal InAlN material, giving rise to unwanted characteristics. The bandgap has a strong dependence on composition, which determines the emission wavelength and efficiency of an optoelectronic device.

Ga auto-incorporation can be difficult to determine through x-ray diffraction (XRD) alone, which is often the primary measurement of composition and structural quality after growth. This is

* Corresponding author.
E-mail address: elaine.taylor@strath.ac.uk (E. Taylor).

http://dx.doi.org/10.1016/j.jcrysgro.2014.09.031
0022-0248/© 2014 The Authors. Published by Elsevier B.V. This is an open access article under the CC BY license (http://creativecommons.org/licenses/by/3.0/).

due to the interplay of composition and strain, and therefore Ga inclusion can often be missed. In this work we present a thorough analysis of the composition of Ga auto-incorporated InAlGaN layers using wavelength dispersive x-ray (WDX) spectroscopy, Rutherford backscattering spectrometry (RBS) and x-ray diffraction (XRD) techniques. The optical properties of these InAlGaN layers are also investigated using cathodoluminescence (CL) measurements and related to the compositional data.

2. Experimental details

Nominally InAlN (80 nm) layers were deposited on 2 μm GaN buffer layers in a 3 × 2 in AIXTRON close coupled showerhead MOCVD reactor, using 0.4° miscut sapphire substrates. All layers were non-intentionally doped. Between each growth the reactor was thermally baked at 1200 °C (susceptor surface temperature) followed by a brush clean of the showerhead to minimise epilayer cross-run contamination. Trimethylgallium (TMGa), trimethylindium (TMIn) and trimethylaluminium (TMAl) were used as group III precursors. The GaN layers used a standard recipe with a substrate thermal clean at 1100 °C followed by a low temperature GaN nucleation layer. The GaN buffer growth was undertaken at 1060 °C with H_2 used as a carrier gas. A standard nucleation-coalescence approach [12] was used where the pressure during the first 1.5 μm was kept at 300 mbar, and then was decreased to 150 mbar for the last 0.5 μm. The TMGa flow was set at 111 μmol/min resulting in a growth rate of 0.67 nm/s at a V/III ratio of 1166 (2900 sccm of NH_3). The total flow through the reactor was 8000 sccm for the GaN growth. While keeping the same showerhead-to-susceptor gap of 11 mm, other growth conditions were then changed to those suitable for InAlN growth, with N_2 carrier gas both for the main reactor flow and as the precursor flow for TMAl and TMIn. The InAlN epilayer growth parameters are presented in Table 1. Sample B has three times the group III and V precursor flows of sample A, and the carrier flows are scaled up accordingly to give a total flow of 24 000 standard cubic centimetres per minute (sccm) compared to 8000 sccm for A. Sample C uses the same group III and V precursor flow rates as A but maintains the high 24 000 sccm total flow rate of sample B, by using an increased carrier gas flow. As a result the V/III ratio of 5481 was held the same for all samples, as was the temperature (790 °C) and the total pressure (70 mbar). Due to the slower growth rate in the case of sample C one would expect a lower nominal In composition due to expected desorption during growth.

WDX measurements were taken in a Cameca SX100 electron probe micro-analyser (EPMA) consisting of three x-ray spectrometers with TAP (thallium acid phthalate), LPET (large pentaerythritol) and PC1 (synthetic pseudocrystal) diffracting crystals used for elemental detection [13,14]. RBS measurements were performed using a collimated beam of 2 MeV He^+ ions and a silicon pin diode detector positioned at a scattering angle of 165°. Spectral fitting of the RBS data was performed manually [15] and then confirmed by “Nuno's Data Furnace” (NDF) code fitting [16] to obtain composition and thickness information. X-ray diffraction (XRD) data was measured using a PanAnalytical X'Pert double crystal diffractometer. Taken together the techniques provide information on composition, spatial homogeneity, depth homogeneity and strain. The optical properties of the layers were investigated using cathodoluminescence (CL) measured in a scanning electron microscope [17,18].

Table 1
Selected growth parameters for the nominal InAlN epilayers grown in this series.

InAlN layer growth condition	Sample A	Sample B	Sample C
NH_3 (mmol/min)	56	168	56
TMIn (μmol/min)	5	16	5
TMAl (μmol/min)	5	16	5
Growth time (s)	1330	1300	2520
Reactor total flow (sccm)	8000	24 000	24 000

3. Results and discussion

Qualitative WDX spectral scans were performed at various electron beam energies to detect all elements present within the nominal InAlN/GaN bilayers. Each WDX crystal is rotated over the full angular range and maxima are detected at the corresponding element x-ray wavelength satisfying Bragg's law. The main x-ray lines detected were In Lα, Al Kα, Ga Lα and N Kα. At a beam energy of 2 keV a Monte Carlo electron trajectory simulation [19] shows that 90% of the deposited energy is within 35 nm as shown in Fig. 1(a). Fig. 1(b) shows a Ga peak in the spectrum from the TAP crystal at 2 keV, for which the beam excitation volume does not penetrate into the underlying GaN, demonstrating the presence of Ga within the top layer.

The threshold energy for excitation of the indium Lα x-ray is approximately 3.5 keV, requiring an electron beam energy in excess of this to accurately measure the In content. Analysis of electron trajectories using Monte Carlo simulations indicates that the excitation volume for beam energy of 4 keV reaches to a depth of approximately 95 nm for InAlGaN on GaN. Thus the thickness of the studied layers ($<$ 90 nm) is such that electrons of energy 4 keV and higher will penetrate through to the underlying GaN layer and generate x-rays from here (Fig. 1). Measurements were therefore taken at a number of different beam energies in the range of 2–6 keV and the composition determined using software that analyses x-ray fluorescence from multilayer structures [20]. An InAlGaN–GaN bilayer was simulated for various (stoichiometric) quaternary compositions with the thickness of the quaternary

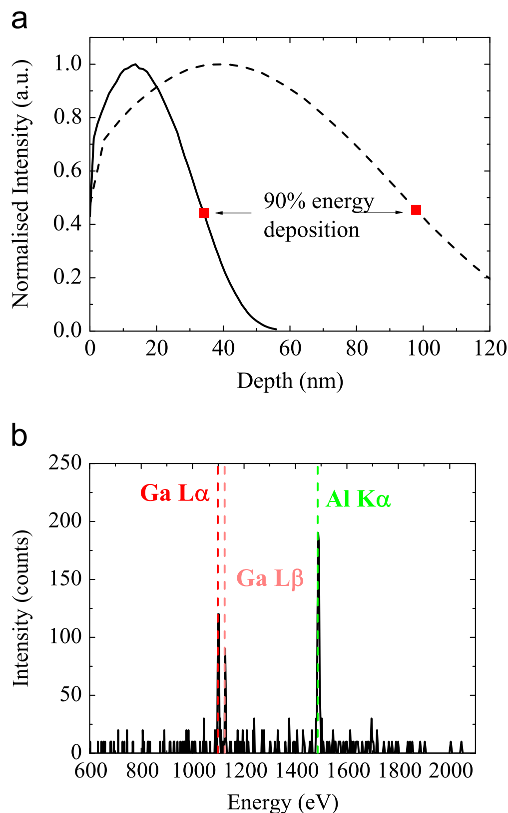

Fig. 1. (a) Beam energy deposition from Monte Carlo electron trajectory simulations of 2 keV (solid line) and 4 keV (dashed line) beam energies. (b) Example WDX spectrum from the TAP crystal using a 2 keV beam showing the presence of Ga.

layer set to be that determined from XRD. Characteristic x-ray fluorescence intensities were measured and compared with those from known standards (AlN for Al, InP for In and GaN for Ga and N). The InAlGaN composition was altered in the simulation to provide an optimum fit to the measured WDX data as a function of excitation energy. The WDX data for In, Ga and Al are plotted against electron beam energies in Fig. 2 for sample A. The decrease in Al and In counts and the increase in Ga at higher beam energies are due to the excitation volume penetrating further into the underlying GaN. For energies below the In $L\alpha$ x-ray excitation energy there are no In counts, whilst the Ga counts measured below 3 keV confirm the presence of Ga in the upper layers. The fractional error in fitting to the measured points was calculated for each element at each beam energy. These values were averaged over the 15 points to obtain the uncertainty in the fit for each sample. Combining the error in the fit with the random and systematic errors resulted in fractional uncertainties of approximately 10% (i.e. [InN] = 7.0 ± 0.7).

RBS measurements were performed on each of the samples to confirm Ga auto-incorporation. To determine the composition and estimate its uncertainty, a manual analysis of the spectra was performed with the assumption of a homogeneous quaternary layer and a III/V ratio of unity. For this the Al/In and the Ga/In ratios were determined from signal areas and heights, respectively, following the procedures in Refs. [15,21]. Furthermore, the data was fitted using the “NDF” code [16] confirming the compositional results and yielding values for the film thicknesses. Fig. 3 shows the RBS spectrum measured from sample A and the corresponding fit assuming a homogeneous quaternary film. The Ga-incorporation in the uppermost layer is clearly shown by the shoulder at 1600 keV. Fig. 3 shows the RBS of all samples in the relevant area comprising the signals of In and Ga close to the surface. Incorporation of Ga is clearly observed for all samples albeit with different concentrations. The overall fractional uncertainty associated with the RBS data for the In and the Ga content is approximately 4%, and the Al content approximately 1%.

The resulting WDX and RBS compositional data for the upper layer are summarised in Table 2, and reveal GaN fractions between 12% and 24% and InN fractions between 7% and 15%. There is a high degree of consistency between the WDX and RBS techniques. Consistently the RBS estimate of the InAlGaN thickness is somewhat lower than that determined by XRD. This could be a combined result of measuring different areas of the wafer (i.e. centre and edge) or small discrepancies between the techniques, with the XRD thickness determined from the Pendellösung fringes and the RBS thickness calculated using a density determined from interpolation of the known density values of the III-N binaries.

Relating these compositional results back to the growth parameters we can see that those for sample A have resulted in more Ga incorporation, compared to samples B and C. This indicates that an increase in total flow rate acts to suppress the Ga incorporation. This dependence is not explored in other reports [9–11], where the precursor flow rates have either been fixed, or varied individually. For example an increase in TMIn alone was shown to influence the Ga incorporation in Ref. [11]. Our result clearly indicates that the auto-incorporation is due to residual Ga coming from the reactor walls and delivery pipes, in agreement with Refs. [9,11] but differs to the conclusion in Ref. [10]. Increasing the total flow rate causes a reduction in the concentration of Ga above the sample surface, assuming a constant supply of Ga from the reactor walls and pipes. Sample C has approximately half the growth rate of samples A and B, but the results show no dependence on Ga auto-incorporation on growth rate.

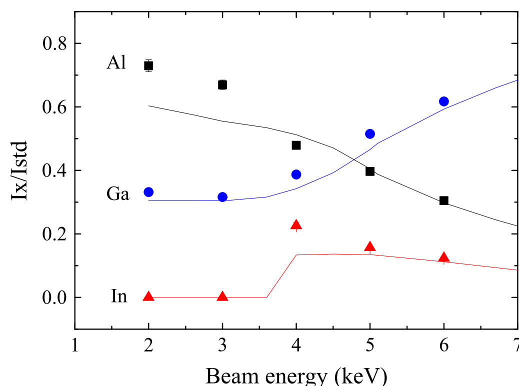

Fig. 2. WDX measurement (points) and simulation (lines) for sample A.

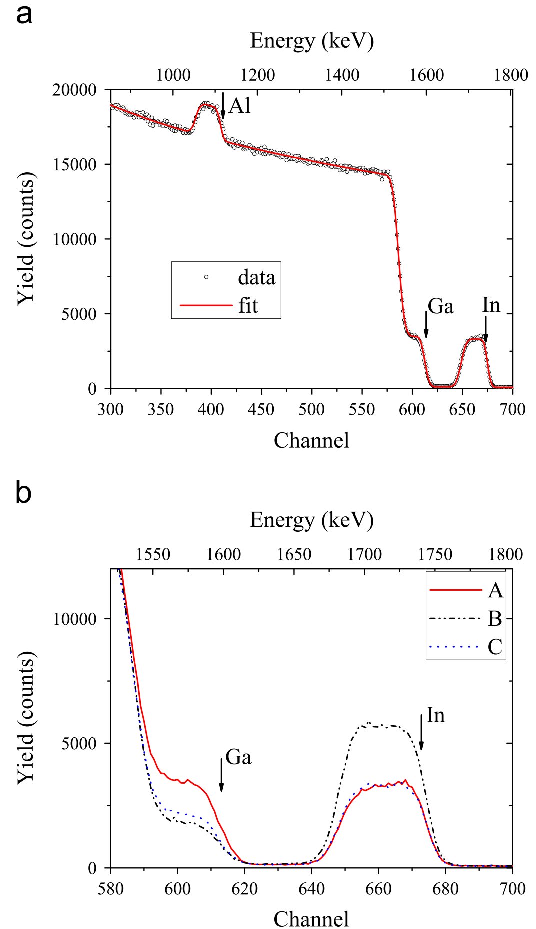

Fig. 3. (a) RBS plot of the InAlGaN layer on GaN of sample A, showing the aluminium, gallium and indium signals. (b) Measured RBS of all samples highlighting the small shoulder at ~1600 keV due to Ga in the top layer. Arrows indicate elements at the surface.

Table 2
Composition fraction results from WDX and RBS measurements, checked for consistency by XRD, and the *a* and *c* lattice parameters for the InAlGaN layer calculated from reciprocal space maps using 10^{-15} XRD scans.

	Sample A		Sample B		Sample C	
	WDX	RBS	WDX	RBS	WDX	RBS
AlN (%)	69.0	72.2	73.0	74.9	79.0	79.7
InN (%)	7.0	7.9	15.0	14.4	7.0	8.0
GaN (%)	24.0	19.9	12.0	10.7	14.0	12.3
XRD thickness (nm)	87.5		82		88	
RBS thickness (nm)	79		79		81	
InAlGaN *a* (Å)	3.178		3.174		3.199	
InAlGaN *c* (Å)	5.072		5.116		5.046	

A reciprocal space map was measured using 10^{-15} XRD scans to provide strain information for each sample. All InAlGaN layers were found to be fully strained to the underlying GaN, having the same *a* lattice parameter as shown for sample A in Fig. 4. The InAlGaN *c* lattice parameter varied across the sample set from 5.046 to 5.116 Å, as shown in Table 2. The *c* lattice parameters calculated from the compositional results using the Vegard law are in good agreement with these RSM values, increasing in the order samples C, A, and B. Sample B, with the considerably higher InN content, is seen to have the highest *c*-parameter and thus the lowest level of in-plane strain. All the allowed composition and relaxation values for the 0002 scans of each InAlGaN sample were determined using this strain data. Both the WDX and RBS measured compositions for all samples fell within the range of determined XRD compositions providing further consistency between the techniques. The XRD analysis and further strain and structural investigations are presented in Smith et al. [22].

The optical properties of these InAlGaN epilayers were studied using CL. Fig. 5 shows CL spectra measured using a 5 kV beam voltage. These spectra are the mean of the 10^4 spectra in 5 μm^2 hyperspectral maps consisting of 100×100 pixels with a full spectrum saved at each pixel. The CL maps reveal a strong GaN peak at 3.4 eV which comes from the underlying GaN buffer layer. A broad InAlGaN luminescence band is also evident within the maps and is fairly uniform over the mapped area, with several single spectra from different areas seen to have minimal change in shape. The InAlGaN luminescence of sample B is red shifted (3.7 eV) in comparison to samples A and C (3.95 eV). This is due to the higher InN content (15%) within the layer. Sample A has 10% more GaN than sample C but has comparable spectra and the same peak energy which indicates that the change in GaN content has no great effect on the luminescence peak energy. This is the result of the extreme bandgap bowing for InAlN at low InN contents, which reduces the possible bandgap variation for InAlGaN as the GaN content changes at low InN [23].

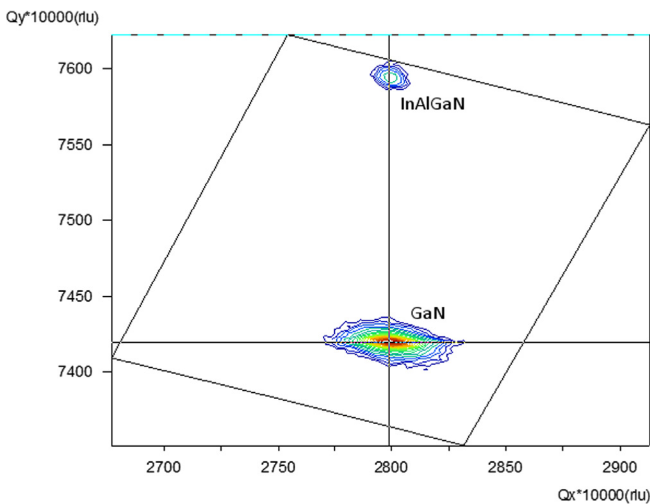

Fig. 4. 10^{-15} RSM of sample A illustrating fully strained layer.

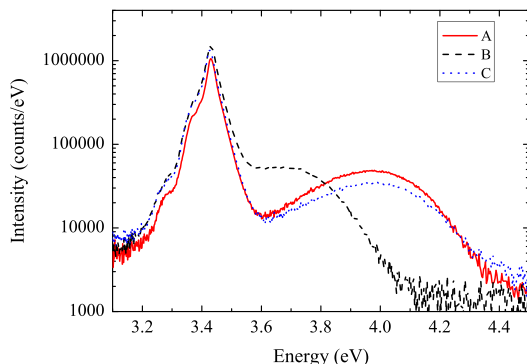

Fig. 5. Mean spectra of CL maps show the InAlGaN luminescence peak.

4. Conclusions

The composition and optical properties of a set of InAlGaN with Ga auto-incorporation have been analysed. Composition measurements from different techniques confirm the presence of Ga within the epilayer and the values returned are all in good agreement. The growth parameters and the resultant Ga incorporation indicate the likely cause being residual Ga coming from the reactor walls and delivery pipes. Increasing the total flow rate from 8000 sccm to 24 000 sccm is seen to suppress the GaN incorporation from 24% to 12%. Luminescence measurements revealed a broad InAlGaN peak whose energy varies with InN composition but not with the change in GaN.

Acknowledgements

We are grateful to Vitaly Zubialevich for useful discussions. We acknowledge funding from the UK Engineering and Physical Sciences Research Council (EPSRC, Grant nos. EP/I012591/1 and EP/I029141/1), European Space Agency (ESA), Science Foundation Ireland (Grant nos. 10/IN.1/I2993 and 07/EN/E001A), and FCT Portugal (Grant PTDC/FIS-NAN/0973/2012 and “Investigador FCT”). M.D.S. and T.C.S. acknowledge the Irish Research Council for their studentship and postdoctoral fellowship, respectively. M.D.S. acknowledges studentship co-funding from ESA. This work was conducted under the framework of the Irish Government's Programme for Research in Third Level Institution Cycles 4 and 5, National Development Plan 2007–2013 with the assistance of the European Regional Development Fund “INSPIRE”. Data associated with research published in this paper can be accessed by contacting the corresponding author.

References

[1] R. Butté, J.-F. Carlin, E. Feltin, M. Gonschorek, S. Nicolas, G. Christmann, D. Simeonov, A. Castiglia, J. Dorsaz, H.J. Buehlmann, S. Christopoulos, G. Baldassarri Höger van Högersthal, A.J.D. Grundy, M. Mosca, C. Pinquier, M.A. Py, F. Demangeot, J. Frandon, P.G. Lagoudakis, J.J. Baumberg, N. Grandjean, Current status of AlInN layers lattice-matched to GaN for photonics and electronics, J. Phys. D: Appl. Phys. 40 (2007) 6328–6344.

[2] K. Lorenz, N. Franco, E. Alves, I.M. Watson, R.W. Martin, K.P. O'Donnell, Anomalous ion channeling in AlInN/GaN bilayers: determination of the strain state, Phys. Rev. Lett. 97 (2006) 085501.

[3] J.-P. Ahl, J. Hertkorn, H. Koch, B. Galler, B. Michel, M. Binder, B. Holländer, Morphology, growth mode and indium incorporation of MOVPE grown InGaN and AlInGaN: a comparison, J. Cryst. Growth 398 (0) (2014) 33–39.

[4] O. Jardel, G. Callet, J. Dufraisse, M. Piazza, N. Sarazin, E. Chartier, M. Oualli, R. Aubry, T. Reveyrand, J.C. Jacquet, M.A. Di Forte Poisson, E. Morvan, S. Piotrowicz, S.L. Delage, Electrical performances of AlInN/GaN HEMTs. A comparison with AlGaN/GaN HEMTs with similar technological process, Int. J. Microw. Wirel. Technol. 3 (2011) 301–309.

[5] S. Guo, X. Gao, D. Gorka, J.W. Chung, H. Wang, T. Palacios, A. Crespo, J.K. Gillespie, K. Chabak, M. Trejo, V. Miller, M. Bellot, G. Via, M. Kossler, H. Smith, D. Tomich, AlInN HEMT grown on SiC by metalorganic vapor phase epitaxy for millimeter-wave applications, Phys. Status Solidi C 207 (6) (2010) 1348–1352.

[6] F. Medjdoub, J.-F. Carlin, M. Gonschorek, M.A. Py, N. Grandjean, S. Vandenbrouck, C. Gaquiere, J.C. DeJaeger, E. Kohn, Small-signal characteristics of AlInN/GaN HEMTs, Electron. Lett. 42 (13) (2006) 779–780.

[7] D. Maier, M. Alomari, N. Grandjean, J. Carlin, M. Diforte-Poisson, C. Dua, S. Delage, E. Kohn, InAlN/GaN HEMTs for operation in the 100 °C regime: a first experiment, IEEE Electron. Device Lett. 33 (7) (2012) 985–987.

[8] I.M. Watson, C. Liu, E. Gu, M.D. Dawson, P.R. Edwards, R.W. Martin, Use of AlInN layers in optical monitoring of growth of GaN-based structures on free-standing GaN substrates, Appl. Phys. Lett. 87 (15) (2005).
[9] J. Kim, Z. Lochner, M.H. Ji, S. Choi, H.J. Kim, J.S. Kim, R.D. Dupuis, A.M. Fischer, R. Juday, Y. Huang, T. Li, J.Y. Huang, F.A. Ponce, J.H. Ryou, Origins of unintentional incorporation of gallium in InAlN layers during epitaxial growth: Part II: effects of underlying layers and growth chamber conditions, J. Cryst. Growth 388 (0) (2014) 143–149.
[10] J.J. Zhu, Y.M. Fan, H. Zhang, G.J. Lu, H. Wang, D.G. Zhao, D.S. Jiang, Z.S. Liu, S.M. Zhang, G.F. Chen, B.S. Zhang, H. Yang, Contribution of GaN template to the unexpected Ga atoms incorporated into AlInN epilayers grown under an indium-very-rich condition by metalorganic chemical vapor deposition (MOCVD), J. Cryst. Growth 348 (1) (2012) 25–30.
[11] M. Hiroki, Y. Oda, N. Watanabe, N. Maeda, H. Yokoyama, K. Kumakura, H. Yamamoto, Unintentional Ga incorporation in metalorganic vapor phase epitaxy of In-containing iii-nitride semiconductors, J. Cryst. Growth 382 (0) (2013) 36–40.
[12] S. Figge, T. Böttcher, S. Einfeldt, D. Hommel, In situ and ex situ evaluation of the film coalescence for GaN growth on GaN nucleation layers, J. Cryst. Growth 221 (2000) 262–266.
[13] E. Taylor, F. Fang, F. Oehler, P.R. Edwards, M.J. Kappers, K. Lorenz, E. Alves, C. McAleese, C.J. Humphreys, R.W. Martin, Composition and luminescence studies of InGaN epilayers grown at different hydrogen flow rates, Semicond. Sci. Technol. 28 (6) (2013) 065011.
[14] K.P. O'Donnell, I. Fernandez-Torrente, P.R. Edwards, R.W. Martin, The composition dependence of the $In_xGa_{1-x}N$ bandgap, J. Cryst. Growth 269 (1) (2004) 100–105.
[15] S. Magalhães, N.P. Barradas, E. Alves, I.M. Watson, K. Lorenz, High precision determination of the InN content of $Al_{1-x}In_xN$ thin films by Rutherford backscattering spectrometry, Nucl. Instrum. Methods B 273 (0) (2012) 105–108.
[16] N.P. Barradas, C. Jeynes, Advanced physics and algorithms in the IBA datafurnace, Nucl. Instrum. Methods B 266 (8) (2008) 1875–1879.
[17] P.R. Edwards, R.W. Martin, Cathodoluminescence nano-characterization of semiconductors, Semicond. Sci. Technol. 26 (2011) 064005.
[18] K. Bejtka, P.R. Edwards, R.W. Martin, S. Fernández-Garrido, E. Calleja, Composition and luminescence of AlInGaN layers grown by plasma-assisted molecular beam epitaxy, J. Appl. Phys. 104 (7) (2008).
[19] D. Drouin, A. Couture, D. Joly, X. Tastet, V. Aimez, R. Gauvin, CASINO V2.42A fast and easy-to-use modeling tool for scanning electron microscopy and microanalysis users, Scanning 29 (3) (2007) 92–101.
[20] D. Amabile, R.W. Martin, T. Wang, M.A. Whitehead, P.J. Parbrook, Compositional analysis of AlInGaN quaternary layers grown by metalorganic vapour phase epitaxy, Phys. Status Solidi C 0 (7) (2003) 2478–2481.
[21] C. Jeynes, Z.H. Jafri, R.P. Webb, A.C. Kimber, M.J. Ashwin, Accurate RBS measurements of the indium content of InGaAs thin films, Surf. Interface Anal. 25 (4) (1997) 254–260.
[22] M.D. Smith, E. Taylor, T.C. Sadler, V.Z. Zubialevich, K. Lorenz, H.N. Li, J. O'Connell, E. Alves, J.D. Holmes, R.W. Martin, P.J. Parbrook, Determination of Ga auto-incorporation in nominal InAlN epilayers grown by MOCVD, J. Mater. Chem. C 2 (2014) 5787–5792.
[23] S. Schulz, M.A. Caro, L.T. Tan, P.J. Parbrook, R.W. Martin, E.P. O'Reilly, Composition-dependent band gap and band-edge bowing in AlInN: a combined theoretical and experimental study, Appl. Phys. Express 6 (12) (2013) 121001.